RESEARCH ARTICLE | JANUARY 21 2025

Corroborating the magnetic easy axis of epitaxial (100) α-iron and (0001) $BaFe_{12}O_{19}$ thin films by ^{57}Fe Mössbauer spectroscopy

Y. E. Li ; J. Shine ; C. Guguschev ; M. Brützam; D. G. Schlom ; N. Ravi

AIP Advances 15, 015323 (2025)
https://doi.org/10.1063/5.0244334
CHORUS

Corroborating the magnetic easy axis of epitaxial (100) α-iron and (0001) $BaFe_{12}O_{19}$ thin films by ^{57}Fe Mössbauer spectroscopy

Cite as: AIP Advances 15, 015323 (2025); doi: 10.1063/5.0244334
Submitted: 29 October 2024 • Accepted: 2 January 2025 •
Published Online: 21 January 2025

Y. E. Li,[1] J. Shine,[2] C. Guguschev,[3] M. Brützam,[3] D. G. Schlom,[1,3,4,a)] and N. Ravi[2,b)]

AFFILIATIONS

[1] Department of Materials Science and Engineering, Cornell University, Ithaca, New York 14853, USA
[2] Physics Department, Spelman College, Atlanta, Georgia 30314, USA
[3] Leibniz-Institut für Kristallzüchtung, Max-Born-Str. 2, 12489 Berlin, Germany
[4] Kavli Institute at Cornell for Nanoscale Science, Ithaca, New York 14853, USA

[a)] **Author to whom correspondence should be addressed:** schlom@cornell.edu
[b)] **E-mail:** nravi@spelman.edu

ABSTRACT

60 and 120 nm thick epitaxial films of isotopically enriched bcc iron (α-^{57}Fe) grown on (100) MgO substrates are studied using x-ray diffraction, reflection high-energy electron diffraction (RHEED), and conversion electron Mössbauer spectroscopy (CEMS). X-ray diffraction and RHEED data indicate that each film behaves as a single crystal material consistent with the relative intensity ratios of the spectral lines observed in the CEMS spectrum. Data further confirm that the easy axis of magnetization lies along the ⟨100⟩ family of directions of the cubic α-iron film. The relevant theory to understand the relative intensities in a magnetic Mössbauer spectrum is outlined and is applied to interpret the intensity ratio of the Mössbauer spectral lines of a more complex hexaferrite magnetic system, $BaFe_{12}O_{19}$, grown on a single crystal substrate of $Sr_{1.03}Ga_{10.81}Mg_{0.58}Zr_{0.58}O_{19}$. The conclusion that the magnetic moment in (0001)-oriented epitaxial $BaFe_{12}O_{19}$ film lies perpendicular to the plane of the substrate is deduced from the absence of the second and fifth lines by comparing the CEMS spectrum of the epitaxial (0001) $BaFe_{12}O_{19}$ film with the spectrum of a polycrystalline $BaFe_{12}O_{19}$ powder. Our measurements using CEMS corroborate what is known about the direction of the magnetic easy axis in α-iron and $BaFe_{12}O_{19}$ and motivate the use of CEMS to probe more complex atomically engineered epitaxial heterostructures, including superlattices.

INTRODUCTION

There has been enormous interest in understanding the magnetic and electrical properties of nanoscale materials. This understanding is gained using a variety of tools such as magnetic force microscopy (MFM), photoelectron spectroscopy (PES), and magnetic circular dichroism (MCD).[1–3] In addition, for Fe-containing systems, ^{57}Fe Mössbauer spectroscopy has proven to be a very useful tool to probe the iron nucleus to get insight into the nature of the charge distribution and the origin of the internal magnetic field. The technique offers very high precision in measuring interaction energies on the order of 4.8×10^{-10} eV and is, therefore, suitable for studying hyperfine interactions due to electron–nucleus interactions in materials.

In ^{57}Fe Mössbauer spectroscopy, a precursor radioactive source, ^{57}Co, in a metal matrix, emits by an electron capture process a recoilless γ-ray with an energy of 14.4 keV, corresponding to the transition energy for an iron nucleus between its nuclear ground and first excited states. The photon transmitted by the material is counted by standard methods in the conventional transmission geometry. Alternatively, if the material under study is so thin that the transmission mode does not yield discernible results due to weak absorption, a backscattering geometry is employed. This makes the backscattering geometry conducive to studying thin films of materials that are grown in polycrystalline or epitaxial form by methods such as DC sputtering.

In the backscattering geometry, conversion electron Mössbauer spectroscopy (CEMS) is particularly well suited for the study of thin

films. In CEMS, the absorbed recoilless photon undergoes a decay process by knocking off the 7.3 keV K-electron of the iron atom. The emitted *K*-electrons reaching the surface are counted by a suitable detector. It should be pointed out that the electrons that make it to the surface for counting come from the top few hundred nanometers of thickness only. In addition, it is known that the internal conversion coefficient for the conversion electron process is ~0.9 (90%), which means for every 100 absorbed photons, ~90 *K*-electrons are generated.[4–6]

We are engaged in the study of iron-based thin films grown on suitable substrates by molecular-beam epitaxy (MBE), including $Fe_{1-x}Ga_x$,[7,8] $BiFeO_3$,[9,10] hexagonal $LuFeO_3$,[11] hexagonal $ScFeO_3$,[12] $LuFe_2O_4$,[13] $DyFe_2O_4$,[14] $Lu_3Fe_5O_{12}$,[15] and superlattices involving these phases.[16–18] As the first step of a larger study involving the use of ^{57}Fe CEMS to characterize epitaxial films, we grew pure, epitaxial, (100)-oriented α-iron on a (100) MgO substrate, as pure iron is used as a calibration standard in ^{57}Fe Mössbauer spectroscopy, especially in the transmission mode. It is common knowledge that pure elemental bcc iron metal (α-iron) is a ferromagnetic material at room temperature. Extensive studies related to the ferromagnetic properties of iron, viz., magnetic susceptibility, neutron scattering, and ^{57}Fe Mössbauer spectroscopy, are available in the literature.[19,20] We explored the study of thin films of pure α-iron using the CEMS technique. As a part of our ongoing study on thin-films, we describe in this paper the usefulness of the CEMS technique to study epitaxial α-iron grown on MgO substrates and epitaxial $BaFe_{12}O_{19}$ grown on $Sr_{1.03}Ga_{10.81}Mg_{0.58}Zr_{0.58}O_{19}$ (SGMZ) substrates.[21]

EXPERIMENTAL

Epitaxial single crystalline α-iron films are grown in a Veeco Gen 10 MBE system. A molecular beam of iron is generated by loading a mixture of 5.00 g of 95.6% enriched ^{57}Fe metal sheets and 11.5 g of unenriched iron metal sheets (which contain 2.12% ^{57}Fe) into a 40 cc alumina crucible, which is in turn placed in an MBE effusion cell and heated. The resulting iron molecular beam has a ~30% ^{57}Fe composition. The flux of the iron molecular beam is measured to be $5.30 \times 10^{13}/(cm^2 \cdot s)$ by a quartz crystal microbalance (QCM) at an iron source temperature of 1260 °C. With this flux, the growth rate of epitaxial (100) α-iron on (100) MgO substrate is calculated to be about 22.5 nm per hour. Two epitaxial (100) α-iron films are then grown on (100) MgO substrates with a base pressure of 3×10^{-8} Torr and a substrate temperature of 405 °C measured by a thermocouple placed between the SiC heater and the substrate. The growth of the two films is timed so that they are about 60 and 120 nm thick, respectively. *In situ* reflection high-energy electron diffraction (RHEED) patterns are recorded using KSA-400 software from k-Space Associates and a Staib electron source operated at 13 kV and a filament current of 1.5 A. Following iron growth, the sample is cooled down to room temperature, and a ~50 nm thick aluminum capping layer is deposited on top to protect the iron films from being oxidized over time in air.

A 120 nm thick $BaFe_{12}O_{19}$ film is also grown in the Veeco Gen 10 MBE system by co-deposition of iron and barium on a (0001) SGMZ substrate, at a substrate temperature of 790 °C measured by an optical pyrometer operating at a wavelength of 1550 nm. Distilled ozone (~80% O_3 + 20% O_2) is used as the oxidant and the background pressure of this oxidant is 1×10^{-6} Torr during growth. The iron flux is$3.50 \times 10^{13}/(cm^2 \cdot s)$, which evaporates from the same isotopically enriched ~30% ^{57}Fe source. The barium flux is 2.92 $\times 10^{12}/(cm^2 \cdot s)$. With these fluxes, the growth rate of the epitaxial (0001) $BaFe_{12}O_{19}$ on (0001) SGMZ substrate is calculated to be about 36.7 nm per hour. *In situ* RHEED patterns are also recorded using KSA-400 software and a Staib electron source operated at 13 kV and a filament current of 1.5 A.

X-ray diffraction (XRD) scans of epitaxial α-iron and $BaFe_{12}O_{19}$ films are measured with a PANalytical Empyrean diffractometer with Cu $K\alpha_1$ radiation. In addition, an XRD scan of a randomly oriented polycrystalline iron powder (Fischer Scientific purity 99% +) is performed with a Shimadzu XRD-6000 diffractometer, utilizing Cu $K\alpha$ radiation. ^{57}Fe Mössbauer studies are conducted at room temperature using a Web Research Company Mössbauer Spectrometer in conjunction with an Iron Analytics CEMS detector. A 25 mCi ^{57}Co source in a rhodium matrix is employed as the energy source. For the CEMS measurement, the sample is kept inside the detector (acting as cathode) with a constant flow of 90% He/10% CH_4 gas. The flow rate is maintained to be 1 sccm. A high voltage of nearly 1400 V with appropriate gain was applied to the detector. The spectra are analyzed with MossWinn software.[22]

RESULTS AND DISCUSSIONS

During MBE growth, the surface crystal quality of the iron and $BaFe_{12}O_{19}$ films is monitored *in situ* by RHEED. Figures 1(a) and 1(b) show the RHEED images taken at the end of the growth of the 120 nm thick iron film and the 120 nm thick $BaFe_{12}O_{19}$ film. The bright and sharp streaks indicate atomically smooth, single-crystal epitaxial films with high crystallinity. After growth, XRD θ-2θ and ϕ scans were performed on the iron films to determine the crystalline phase and its epitaxial orientation relationship to the (100) MgO substrate. The XRD θ − 2θ scan of the 120 nm thick α-iron film is shown in Fig. 2(a). The Bragg peak seen at 2θ of ~42.8° is attributed to the 200 reflection of the MgO substrate, while the peak at ~65.1° is due to the 200 reflection of the bcc iron (the α-iron phase). The XRD ϕ-scans for the 111 family of reflections of MgO and the 211 family of reflections of bcc iron are plotted together in Fig. 2(b). The MgO 111 peaks are 45° away in ϕ from those of iron 211, meaning iron's [011] in-plane direction is 45° away from MgO's [011] in-plane direction. These XRD results indicate epitaxial growth with an orientation relationship of (100) Fe || (100) MgO with [001] Fe || [011] MgO. This epitaxial orientation relationship is well known from the literature from prior studies in which iron was grown epitaxially on (100) MgO.[23–29] Hence the Fe/MgO system behaves like a single crystal rather than a polycrystalline system. This behavior is substantiated by the CEMS data discussed below. The XRD θ − 2θ scan of the 120 nm thick $BaFe_{12}O_{19}$ film is shown in Fig. 2(c). Observation of multiple 000ℓ reflections, and just 000ℓ reflections, in combination with the RHEED image of Fig. 1(b), confirms that the $BaFe_{12}O_{19}$ epitaxial film is oriented with its (0001) plane parallel to the (0001) plane of the isostructural SGMZ substrate.

The Mössbauer spectrum observed for pure α-iron metal offers insightful information related to the direction of the magnetic

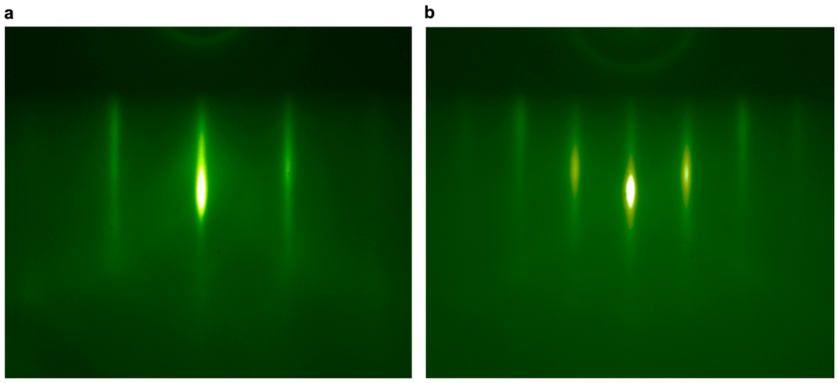

FIG. 1. RHEED images of (a) the 120 nm thick iron film, taken at the end of the growth along the [001] azimuth of the (100) α-iron film [or equivalently along the [011] azimuth of the (100) MgO substrate] and (b) the 120 nm thick $BaFe_{12}O_{19}$ film, taken at the end of the growth along the [110] azimuth of the (0001) $BaFe_{12}O_{19}$ film.

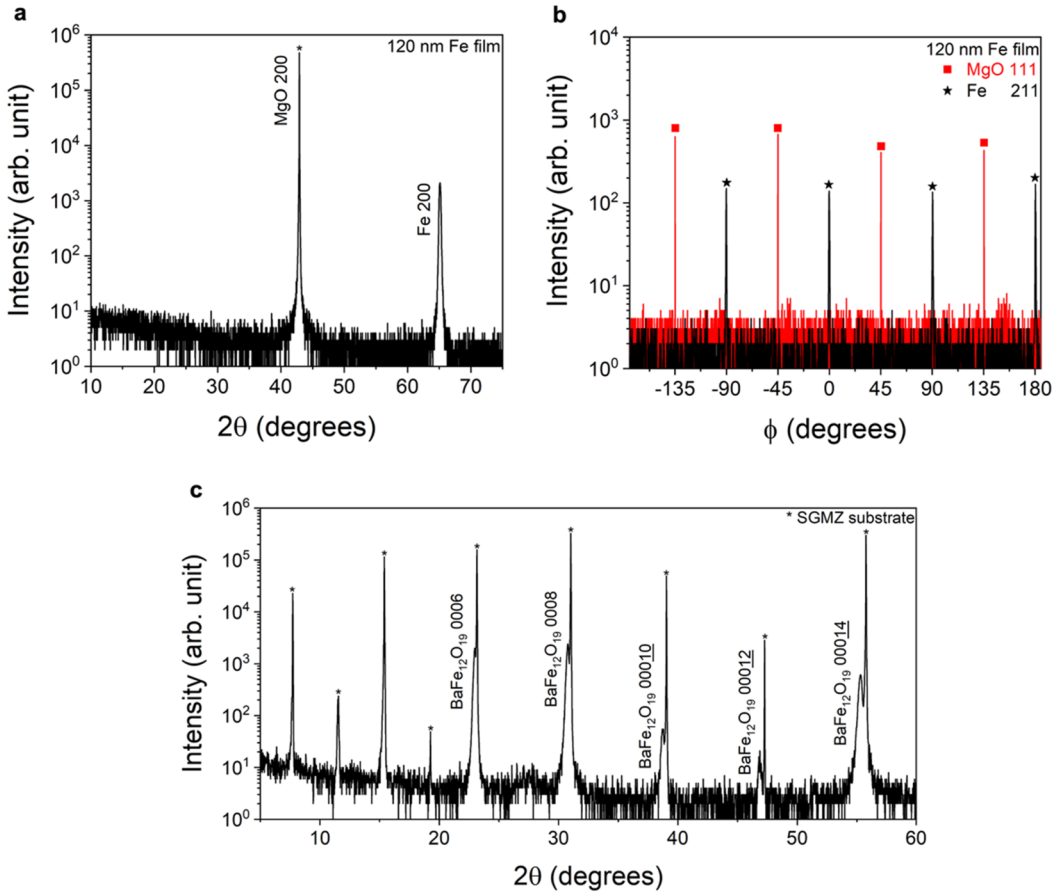

FIG. 2. XRD (a) θ − 2θ scan of the 120 nm thick α-iron film, (b) ϕ-scan of the 120 nm thick α-iron film, and (c) θ − 2θ scan of the 120 nm thick $BaFe_{12}O_{19}$ film.

moment based on the spectral characteristics of the Zeeman magnetic spectrum. Usually, a magnetic spectrum is observed when a material possesses an internal magnetic field, and a typical spectrum is comprised of eight possible spectral transitions arising from the ground state with a nuclear spin of $\boldsymbol{I} = 1/2$ to the first excited state with a nuclear spin of $\boldsymbol{I} = 3/2$. For clarity, the energy level diagram of iron and all the possible transitions are shown in Fig. 3. In the presence of an internal magnetic field, the ground and the first excited states of the ^{57}Fe nuclear energy level are split into two ground states ($m_I = \pm 1/2$) and four excited states ($m_I = \pm 1/2, \pm 3/2$) degenerate energy levels, respectively, following the $(2\boldsymbol{I} + 1)$ energy level expression, where $\boldsymbol{I}$ is the nuclear spin. In other words,

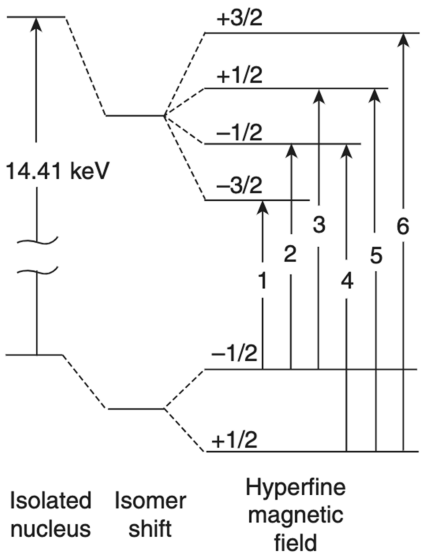

FIG. 3. Energy level scheme for ^{57}Fe. Reproduced with permission from Characterization of Materials, edited by E. Kaufmann (John Wiley, New York, 2012). Copyright 2012 Wiley. Reprinted with permission conveyed through Copyright Clearance Center, Inc.

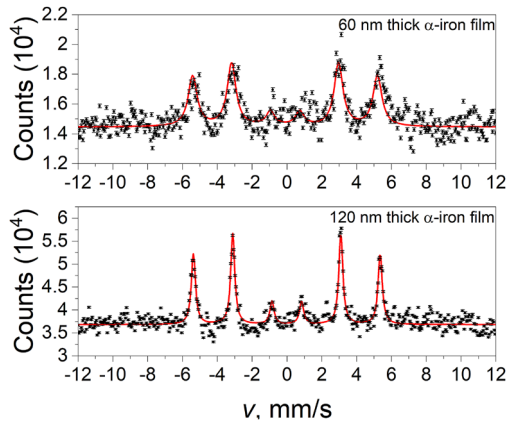

FIG. 4. CEMS data of α-iron films epitaxially grown on (100) MgO. (Top) 60 nm thick film. (Bottom) 120 nm thick film.

the presence of the internal magnetic field lifts the degeneracy to two and four eigenstates for nuclear ground and first excited states, respectively, thus enabling eight possible transitions. Due to parity rules and angular momentum considerations, however, two transitions with $\Delta m_I = \pm 2$ are not allowed, thus making only six transitions possible, unless there is an admixture of eigenstates. In a polycrystalline system such as a powder sample, one encounters all possible orientations of the magnetic moment, and a powder averaging is usually performed to account for the intensity of the observed spectral lines.

The CEMS spectra of the films of Fe/MgO are shown in Fig. 4. An inspection of the data clearly indicates that there are six resonance peaks and the intensities of the second and the fifth lines are larger than those of lines 1 and 6, a behavior atypical of randomly oriented polycrystalline α-iron. This observation is, however, consistent with the fact that the epitaxial α-iron film grown on (100) MgO is a single crystal containing domains in which the ⟨100⟩ directions of the α-iron, which are the easy axis directions of the magnetic moment as determined by magneto-optic Kerr effect (MOKE),[30] vibrating sample magnetometry (VSM),[31] and ferromagnetic resonance (FMR) spectroscopy,[31] are restricted to two specific in-plane directions: the ⟨011⟩ in-plane directions of the (100) MgO substrate. Although the out-of-plane direction of these epitaxial α-iron films is also a ⟨100⟩ direction, the magnetization does not lie in that direction due to shape anisotropy. Instead, it populates only the in-plane ⟨100⟩ directions of the α-iron, which are only along two specific directions of the substrate. This contrasts with randomly oriented polycrystalline α-iron, where the grains exhibit ⟨100⟩ directions in all spatial orientations due to the lack of restrictions by epitaxy.

As the magnetic moment is uniquely aligned in one direction in each domain, it is inferred that the epitaxial film of α-iron behaves like an anisotropic single crystal. This is in accordance with the x-ray data as well. A least-squares fit of the CEMS data, assuming a single-crystal orientation of the magnetic moment with a Lorentzian line function, yields the solid lines drawn on the spectra shown in Fig. 4. A comparison of the CEMS data of the samples shows that the thicker sample displays a sharper line width (0.32 mm/s) than the thinner sample (0.43 mm/s). This behavior is as expected because the thicker sample contains 2.5×10^{17} ^{57}Fe atoms, while the thinner sample has half this value.

The relative intensities of the spectral lines are calculated from the theory of the coupling of two angular momenta of the nuclear ground and excited states of ^{57}Fe. The intensity of the spectral lines is due to an angular-dependent and an angular-independent part, where the angle involved is between incoming γ-rays and the internal magnetic field of the ^{57}Fe atoms. The angular-independent part corresponds to the situation where there is no preferred orientation in the laboratory frame for the appropriate principal axis, which would be the case when the absorber is a non-oriented polycrystalline material. If the γ-ray emission occurs between two energy levels with I_z values of m_1 and m_2, with a net m value of $m_1 + m_2$ corresponding to the nuclear spin $\boldsymbol{I}_1$ and $\boldsymbol{I}_2$ with a $\boldsymbol{J}$ value of $\boldsymbol{I}_1 + \boldsymbol{I}_2$, respectively, then the angular-independent probability term is given by the square of the appropriate Clebsch–Gordon coefficients (C–). Generally, $\boldsymbol{J} = 1$ is classified to be a magnetic dipole transition (M1) due to the absence of any parity change. The isotope decay of ^{57}Co occurs primarily by a dipole-transition mode. In general, while the transition energies are the differences between the eigenvalues of the excited and ground states, the transition probabilities are calculated from the eigenvectors and the C–G coefficients, which are normalized. The relative intensities in a direction (θ, φ) with respect to the z-direction are then

$$P\left(\theta, \varphi; \frac{3}{2}, i; \frac{1}{2}j\right) = \sum_{m'm''} |C^{m_2}_{(\frac{1}{2},j)} C^{m_1}_{(\frac{1}{2},j)} M_{(m_1,m_2)}|^2,$$

$$M(m_1, m_2) = \left\langle \frac{1}{2}, m_2; \boldsymbol{J}, m \middle| \frac{3}{2}, m_1 \right\rangle \boldsymbol{X}^m_J,$$

where the symbol ⟨|⟩ is the C-G coefficient coupling the three vectors $\boldsymbol{I}(1/2)$, $\boldsymbol{J}$, and $\boldsymbol{I}(3/2)$. The vector $\boldsymbol{X}$ is perpendicular to the direction of the γ-ray emission.

For a powder sample, P must be integrated over θ and φ. The intensities are then

$$P\left(\frac{3}{2}, i; \frac{1}{2}, j\right) = \int_{\theta=0}^{\pi} \int_{\varphi=0}^{2\pi} P\left(\theta, \varphi; \frac{3}{2}, i; \frac{1}{2}, j\right) \sin\theta d\theta d\varphi.$$

This integration is performed analytically, giving a final expression (not shown). This procedure is typically known as the powder averaging process.[32–36] After simplification, this integral yields a relative intensity ratio of 3:2:1:1:2:3 for the magnetic sextet in the order of velocity in which they appear in the Mössbauer spectra.[19] The angular-dependent terms are formulated as the radiation probability in a direction θ to the principal axis of the magnetic field. These calculations are performed for all possible angles of magnetization and the incoming 14.4 keV γ-photons from the ^{57}Co/Rh radioactive precursor. In such a situation, the x-ray diffractogram of the powder would reveal reflections from all possible Miller planes that satisfy Bragg's condition. For bcc iron, 200, 211, and 222 reflections will be seen. If, on the other hand, the angle is either 0° or 90°, corresponding to the case where the magnetization is either along or perpendicular to the direction of the incoming γ-photons, the intensity ratio of the spectral lines changes to 3:0:1:1:0:3 and 3:4:1:1:3:4, respectively.[19] Several different conventions are followed in evaluating Clebsch-Gordon coefficients for the coupling of angular momenta, and here we have adopted the convention given in the *Quantum Mechanics* textbook.[33]

The total emitted radiation is given by the product of both terms, which is

$$Intensity \propto \langle I_1 1 - m_1 m | I_2 m_2 \rangle^2 \Theta(J, m).$$

The angular-dependent terms Θ (J, m) given in Table I are derived from the appropriate Hamiltonian used for simulating magnetic Mössbauer spectra.[32]

Based on the theory stated earlier, it is obvious that the relative intensity ratio measured in Fig. 4, which is ~3:4:1:1:4:3, is inconsistent with a randomly oriented sample of α-iron. Rather, this result is fully expected from a single crystal (or a single-crystal film in our case) of α-iron with an angle θ = 90° in the CEMS measurement. In addition, measurements are made on a randomly oriented polycrystalline iron powder (Fischer Scientific purity 99% +) in both transmission and scattering geometries; the spectra are shown in Fig. 5. While the powder is used for collecting the transmission data, a pellet is prepared with about 500 mg of natural Fe powder that is pressed under 4000 psi for the CEMS measurement. The intensity ratio in both transmission and scattering geometry is found to follow nearly 3:2:1:1:2:3, thus establishing the random orientation of the magnetic moment in a completely randomly oriented polycrystalline material (Curie group $\infty\infty m$).[37–39] The random orientation of the grains of iron in the powder was also corroborated by x-ray diffraction on the same polycrystalline iron powder that was used for the Mössbauer measurements. The result is shown

TABLE I. Probabilities of relative intensities for a dipole transition $(\frac{3}{2}, \frac{1}{2})$.

m_2	m_1	m	C–G$^+$	(C–G)[a] Normalized	Θ for $J = 1$	θ = 90°	θ = 0°
+3/2	+1/2	+1	1	3	$1 + \cos^2\theta$	3	6
+1/2	+1/2	0	$(2/3)^{1/2}$	2	$2\sin^2\theta$	4	0
−1/2	+1/2	−1	$(1/3)^{1/2}$	1	$1 + \cos^2\theta$	1	2
−3/2	+1/2	−2	0	0	0	0	0
+3/2	−1/2	+2	0	0	0	0	0
+1/2	−1/2	+1	$(2/3)^{1/2}$	1	$1 + \cos^2\theta$	1	2
−1/2	−1/2	0	$(1/3)^{1/2}$	2	$2\sin^2\theta$	4	0
−3/2	−1/2	−1	1	3	$1 + \cos^2\theta$	3	6

[a]C–G coefficients are calculated using the procedure described in Ref. 31 for $\left\langle \frac{3}{2}, \frac{1}{2}, m_2, m_1 | 1m \right\rangle$ and converted using the relationship, $\left\langle \frac{1}{2}, 1 - m_1 m | \frac{3}{2}, m_2 \right\rangle \frac{1}{(-1)^{m_1 + \frac{1}{2}} \sqrt{\frac{4}{3}}} = \left\langle \frac{3}{2}, \frac{1}{2}, m_2, m_1 | 1m \right\rangle$.

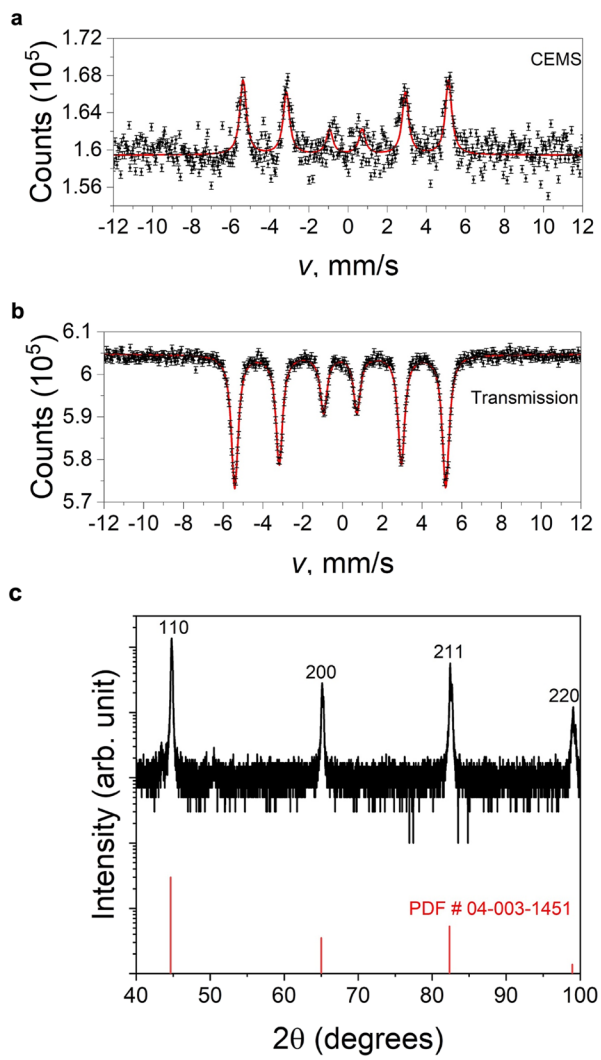

FIG. 5. Mössbauer spectra of the polycrystalline Fe powder. (a) CEMS (pellet), (b) transmission mode (powder), and (c) θ − 2θ scan of the same powder measured in (b) in comparison to a standard (PDF 04-003-1451, Ref. 38) of randomly oriented iron powder.

in Fig. 5(c). All *hkl* peaks of iron are seen, and the intensity ratio between the peaks is in reasonable agreement with what it should be for a randomly oriented powder, as can be seen from the comparison to the intensity ratio reported in PDF 04-003-1451 for iron powder.[40]

Interestingly, CEMS data from a rolled Fe-foil of 30 μm thickness yield an intensity ratio that deviates from a randomly oriented polycrystalline material (see Fig. S1 in the supplementary material), similar to spectra seen in most of the published data on α-iron films on a variety of substrates. This observation illustrates that surface magnetism is somewhat different from that of the bulk material, especially for the rolled films, due to texture (Curie group $\frac{\infty}{m}m$),[37–39] thus confirming a $\infty\infty m$ polycrystalline orientation in the bulk sample and $\frac{\infty}{m}m$ preferred orientation at the surface.[41] It must be borne in mind that for the rolled film/foil, the CEMS technique is sensitive only to layers that are a few hundred nm below the surface of the film, and the magnetic moments of iron atoms in those layers may be aligned differently compared to the bulk material, thus resulting in different intensity ratios in the spectrum attributed to texture effects. Further studies are needed to confirm this idea. Since the direction of the magnetic moment is parallel in-plane in the thin surface of polycrystalline ferromagnetic materials such as an iron foil, the intensity ratio between sextet peaks becomes nearly 3:4:1:1:4:3 when the angle between the γ-ray and the magnetic moment is 90°. It is important to realize that the second and the fifth spectral lines originating from ground states with $m_I = \pm 1/2$ and transitioning to excited states with $m_I = \pm 1/2$ are controlled by the angle between the incident γ-ray and the magnetization axis. In general, one can approximate the relative intensities to be 3:*x*:1:1:*x*:3, and *x* can vary from 0 to 4 depending on the angle.[19,42]

Using the concept enumerated earlier, it is clear that the relative intensities of a magnetic Mössbauer spectrum (transmission or backscattering) depend on the orientation of the magnetic moment of iron. We next extend this concept to a more complex system, $BaFe_{12}O_{19}$, that is currently under study. This magnetic material has four distinct crystallographic sites (Wyckoff positions $4f_1$, $4f_2$, $2a$, and $2b$). An epitaxial $BaFe_{12}O_{19}$ film of thickness 120 nm also enriched with 30% ^{57}Fe was grown on a single-crystal substrate of SGMZ. It displays the complex room-temperature CEMS spectrum shown in Fig. 6. It is apparent that a comparison to the transmission data collected for a powder sample reveals the missing peaks not seen in the film. This film is grown on an SGMZ substrate, and the magnetic moments lie perpendicular to the plane of the substrate, making an angle of 0° with respect to the incoming γ-ray from the radioactive source, resulting in a relative intensity ratio of 3:0:1:1:0:3 (see Table I). A detailed analysis of such a complex magnetic system will be the subject of a future publication. The direction of the easy axis of $BaFe_{12}O_{19}$ inferred from the CEMS measurements is consistent with prior determinations of its easy axis by conventional methods, e.g., by VSM.[43]

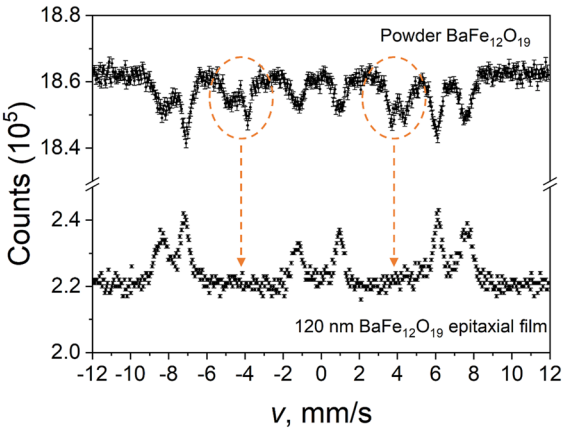

FIG. 6. (Bottom trace) CE Mössbauer spectrum of 120 nm thick epitaxial $BaFe_{12}O_{19}$ film made with 30% ^{57}Fe on a (0001) SGMZ substrate. (Top) Transmission spectrum of powder $BaFe_{12}O_{19}$. The arrows point to the missing peaks not seen in the CEMS spectrum.

CONCLUSIONS

The main conclusions of the present work are summarized as follows:

(a) CEMS is a useful and powerful technique for probing the magnetization properties of complex atomically engineered epitaxial heterostructures, including complex oxides. It provides information on the direction of the easy axis of magnetization in epitaxial films when relative intensities are considered within the theoretical framework.

(b) The obtained information of the epitaxial films is consistent and correlates well with other experimental methods. It is found that the easy axis of magnetization in epitaxial iron on (100) MgO is along the ⟨00⟩ direction, and in $BaFe_{12}O_{19}$ it is perpendicular to the plane of the (0001) SGMZ substrate.

SUPPLEMENTARY MATERIAL

See the supplementary material for the CEMS data of a rolled Fe-foil of 30 μm thickness.

ACKNOWLEDGMENTS

Y.E.L., J.S., D.G.S., and N.R. gratefully acknowledge the support from the National Science Foundation (NSF) through Grant No. DMR-2122147 as well as the Platform for the Accelerated Realization, Analysis, and Discovery of Interface Materials (PARADIMs) under Cooperative Grant Agreement No. DMR-2039380.

AUTHOR DECLARATIONS

Conflict of Interest

The authors have no conflicts to disclose.

Author Contributions

Y. E. Li: Formal analysis (equal); Investigation (equal); Methodology (equal); Writing – review & editing (equal). **J. Shine**: Formal analysis (equal); Investigation (equal). **C. Guguschev**: Conceptualization (equal); Investigation (equal); Resources (equal). **M. Brützam**: Methodology (equal). **D. G. Schlom**: Conceptualization (equal);

Formal analysis (equal); Funding acquisition (equal); Investigation (equal); Methodology (equal); Writing – original draft (equal); Writing – review & editing (equal). **N. Ravi**: Conceptualization (equal); Formal analysis (equal); Funding acquisition (equal); Investigation (equal); Methodology (equal); Writing – original draft (equal); Writing – review & editing (equal).

DATA AVAILABILITY

The data that support the findings of this study are openly available at https://data.paradim.org/doi/0rh9-yn63.

REFERENCES

[1] Y. Takamura, R. V. Chopdekar, A. Scholl, A. Doran, J. A. Liddle, B. Harteneck, and Y. Suzuki, "Tuning magnetic domain structure in nanoscale $La_{0.7}Sr_{0.3}MnO_3$ Islands," Nano Lett. **6**, 1287–1291 (2006).

[2] S. Nishimura, A. T. N. Dao, D. Mott, K. Ebitani, and S. Maenosono, "X-Ray absorption near-edge structure and X-ray photoelectron spectroscopy studies of interfacial charge transfer in gold–silver–gold double-shell nanoparticles," J. Phys. Chem. C **116**, 4511–4516 (2012).

[3] A. E. Sokolov, S. G. Ovchinnikoc, V. N. Sabluda, and A. M. Kal'sin, "Magnetic circular dichroism and the nature of ferromagnetism in colloidal gold nanoparticles," JEPT Lett. **97**, 98–101 (2014).

[4] B. Fultz, "Mössbauer spectrometry," in *Characterization of Materials*, edited by E. Kaufmann (John Wiley, New York, 2012).

[5] J. J. Spijkerman, J. C. Travis, P. A. Pella, and J. R. DeVoe, "Preliminary study on the characteristics and design parameters for a Mössbauer resonant detector," Institute for Materials Research, National Bureau of Standards, Washington, D.C. 20234 Technical Note 541F (1967).

[6] F. Salvat and J. Parellada, "Theory of conversion electron Mössbauer spectroscopy (CEMS)," Nucl. Instrum. Methods Phys. Res., Sect. B **1**, 70–84 (1984).

[7] A. B. Mei, I. Gray, Y. Tang, J. Schubert, D. Werder, J. Bartell, D. C. Ralph, G. D. Fuchs, and D. G. Schlom, "Local photothermal control of phase transitions for on-demand room-temperature rewritable magnetic patterning," Adv. Mater. **32**, 2001080 (2020).

[8] P. B. Meisenheimer, R. A. Steinhardt, S. H. Sung, L. D. Williams, S. Zhuang, M. E. Nowakowski, S. Novakov, M. M. Torunbalci, B. Prasad, C. J. Zollner, Z. Wang, N. M. Dawley, J. Schubert, A. H. Hunter, S. Manipatruni, D. E. Nikonov, I. A. Young, L. Q. Chen, J. Bokor, S. A. Bhave, R. Ramesh, J.-M. Hu, E. Kioupakis, R. Hovden, D. G. Schlom, and J. T. Heron, "Engineering new limits to magnetostriction through metastability in iron-gallium alloys," Nat. Commun. **12**, 2757 (2021).

[9] J. F. Ihlefeld, N. J. Podraza, Z. K. Liu, R. C. Rai, X. Xu, T. Heeg, Y. B. Chen, J. Li, R. W. Collins, J. L. Musfeldt, X. Q. Pan, J. Schubert, R. Ramesh, and D. G. Schlom, "Optical band gap of $BiFeO_3$ grown by molecular-beam epitaxy," Appl. Phys. Lett. **92**, 142908 (2008).

[10] A. B. Mei, Y. Tang, J. Schubert, D. Jena, H. G. Xing, D. C. Ralph, and D. G. Schlom, "Self-assembly and properties of domain walls in $BiFeO_3$ layers grown via molecular-beam epitaxy," APL Mater. **7**, 071101 (2019).

[11] J. A. Moyer, R. Misra, J. A. Mundy, C. M. Brooks, J. T. Heron, D. A. Muller, D. G. Schlom, and P. Schiffer, "Intrinsic magnetic properties of hexagonal $LuFeO_3$ and the effects of nonstoichiometry," APL Mater. **2**, 012106 (2014).

[12] L. M. Garten, Z. Jiang, H. Paik, J. D. Perkins, A. Kakekhani, R. Fei, D. J. Werder, M. E. Holtz, D. S. Ginley, A. M. Rappe, D. G. Schlom, and M. L. Staruch, "Stromataxic stabilization of a metastable layered $ScFeO_3$ polymorph," Chem. Mater. **33**, 7423–7431 (2021).

[13] C. M. Brooks, R. Misra, J. A. Mundy, L. A. Zhang, B. S. Holinsworth, K. R. O'Neal, T. Heeg, W. Zander, J. Schubert, J. L. Musfeldt, Z. K. Liu, D. A. Muller, P. Schiffer, and D. G. Schlom, "The adsorption-controlled growth of $LuFe_2O_4$ by molecular-beam epitaxy," Appl. Phys. Lett. **101**, 132907 (2012).

[14] R. A. Steinhardt, C. M. Brooks, G. C. Correa, M. E. Holtz, R. Ramesh, D. A. Muller, J. A. Mundy, and D. G. Schlom, "$DyFe_2O_4$: A new trigonal rare-earth ferrite grown by molecular-beam epitaxy," APL Mater. **9**, 041106 (2021).

[15] C. L. Jermain, H. Paik, S. V. Aradhya, R. A. Buhrman, D. G. Schlom, and D. C. Ralph, "Low-damping sub-10-nm thin films of lutetium iron garnet grown by molecular-beam epitaxy," Appl. Phys. Lett. **109**, 19240 (2016).

[16] J. A. Mundy, C. M. Brooks, M. E. Holtz, J. A. Moyer, H. Das, A. F. Rébola, J. T. Heron, J. D. Clarkson, S. M. Disseler, Z. Liu, A. Farhan, R. Held, R. Hovden, E. Padgett, Q. Mao, H. Paik, R. Misra, L. F. Kourkoutis, E. Arenholz, A. Scholl, J. A. Borchers, W. D. Ratcliff, R. Ramesh, C. J. Fennie, P. Schiffer, D. A. Muller, and D. G. Schlom, "Atomically engineered ferroic layers yield a room-temperature magnetoelectric multiferroic," Nature **537**, 523–527 (2016).

[17] J. A. Mundy, B. F. Grosso, C. A. Heikes, D. Ferenc Segedin, Z. Wang, Y.-T. Shao, C. Dai, B. H. Goodge, Q. N. Meier, C. T. Nelson, B. Prasad, F. Xue, S. Ganschow, D. A. Muller, L. F. Kourkoutis, L. Q. Chen, W. D. Ratcliff, N. A. Spaldin, R. Ramesh, and D. G. Schlom, "Liberating a hidden antiferroelectric phase with interfacial electrostatic engineering," Sci. Adv. **8**, eabg5860 (2022).

[18] L. Caretta, Y.-T. Shao, J. Yu, A. B. Mei, B. F. Grosso, C. Dai, P. Behera, D. Lee, M. McCarter, E. Parsonnet, K. P. Harikrishnan, F. Xue, X. Guo, E. S. Barnard, S. Ganschow, Z. Hong, A. Raja, L. W. Martin, L. Q. Chen, M. Fiebig, K. Lai, N. A. Spaldin, D. A. Muller, D. G. Schlom, and R. Ramesh, "Nonvolatile electric-field control of inversion symmetry," Nat. Mater. **22**, 207–215 (2023).

[19] N. N. Greenwood and T. C. Gibb, *Mössbauer Spectroscopy* (John Wiley & Sons, 1971).

[20] J. L. Dormann, J. R. Cui, and C. Sella, "Mössbauer studies of Fe_2O_3 antiferromagnetic small particles," J. Appl. Phys. **57**, 4283–4285 (1985).

[21] C. Guguschev, C. Richter, M. Brützam, K. Dadzis, C. Hirschle, T. M. Gesing, M. Schulze, A. Kwasniewski, J. Schreuer, and D. G. Schlom, "Revisiting the growth of large (Mg, Zr):$SrGa_{12}O_{19}$ single crystals: Core formation and its impact on structural homogeneity revealed by correlative X-ray imaging," Cryst. Growth Des. **22**, 2557–2568 (2022).

[22] Z. Klencsar, E. Kuzmann, and A. Vertes, "User-friendly software for Mössbauer spectrum analysis," J. Radioanal. Nucl. Chem. **210**, 105–118 (1996).

[23] H. Sato, R. S. Toth, and R. W. Astrue, "Bitter patterns on single-crystal thin films of iron and nickel," J. Appl. Phys. **33**, 1113–1115 (1962).

[24] K. Thürmer, R. Koch, M. Weber, and K. H. Rieder, "Dynamic evolution of pyramid structures during growth of epitaxial Fe (001) films," Phys. Rev. Lett. **75**, 1767–1770 (1995).

[25] A. Subagyo, H. Oka, G. Eilers, K. Sueoka, and K. Mukasa, "Scanning tunneling microscopy observation of epitaxial bcc-Fe(001) surface," Jpn. J. Appl. Phys. **39**, 3777–3779 (2000).

[26] R. Reitinger, B. Sepiol, G. Vogl, B. Pfau, L.-M. Stadler, S. Stankov, F. Zontone, N. Spiridis, and J. Korecki, "Morphology of Fe/MgO(001) ultrathin films," J. Appl. Phys. **102**, 034310 (2007).

[27] C. Fetzer, I. Dézsi, I. Szűcs, F. Tanczikó, and A. G. Balogh, "The interaction of Fe on MgO(100) surfaces," Surf. Sci. **603**, 3021–3023 (2009).

[28] Q. Zhan, S. Vandezande, K. Temst, and C. Van Haesendonck, "Magnetic anisotropies of epitaxial Fe/MgO(001) films with varying thickness and grown under different conditions," New J. Phys. **11**, 063003 (2009).

[29] B. Blyzniuk, A. Dziwoki, K. Freindl, A. Kozioł-Rachwał, E. Madej, E. Młyńczak, M. Szpytma, D. Wilgocka-Ślezak, J. Korecki, and N. Spiridis, "Magnetization reversal in Fe(001) films grown by magnetic field assisted molecular beam epitaxy," J. Magn. Magn. Mater. **586**, 171151 (2023).

[30] J. L. Costa-Krämer, J. L. Menéndez, A. Cebollada, F. Briones, D. Garca, and A. Hernando, "Magnetization reversal asymmetry in Fe/MgO(001) thin films," J. Magn. Magn. Mater. **210**, 341–348 (2000).

[31] H. Ikeya, Y. Takahashi, N. Inaba, F. Kirino, M. Ohtake, and M. Futamoto, "Magnetic properties of Fe(001) thin films on GaAs(001) deposited by RF magnetron sputtering," J. Phys.: Conf. Ser. **266**, 012116 (2011).

[32] W. Kundig, "Evaluation of Mössbauer spectra for ^{57}Fe," Nucl. Instrum. Methods **48**, 219–228 (1967).

[33] D. H. McIntyre, *Quantum Mechanics* (Pearson, 2012), p. 375.

[34] R. L. Collins, "Mössbauer studies of iron organometallic complexes. IV. Sign of the electric-field gradient in ferrocene," J. Chem. Phys. **42**, 1072–1080 (1965).

[35]N. Ravi and R. Jagannathan, "A Mössbauer study of $FeC_2O_4 \cdot 2D_2O$ below the neel temperature," Hyperfine Interact. **12**, 167–172 (1982).
[36]G. R. Hoy, D. C. Cook, and E. Agyekum, "Feasibility studies of conversion electron mossbauer spectroscopy (CEMS) of iron-doped InP," Technical Report, Naval Research Laboratory Contract No. 100014-83-K2018 (1984).
[37]P. Curie, "Sur la symétrie dans les phénomènes physiques, symétrie d'un champ électrique et d'un champ magnétique," J. Phys. Theor. Appl. **3**, 393–415 (1894).
[38]*International Tables for Crystallography*, 5th ed., edited by T. Hahn (Kluwer, Dordrecht, 2002), Vol. A, pp. 796–799.
[39]M. De Graef and M. E. McHenry, *Structure of Materials: An Lntroduction to Crystallography, Diffraction, and Symmetry* (Cambridge University Press, Cambridge, 2007), pp. 221–222.
[40]S. Gates-Rector and T. Blanton, "The powder diffraction file: A quality materials characterization database," Powder Diffr. **34**, 352–360 (2019).
[41]W. Oester and H. Wever, "Entwicklung von Texturgradienten und Oberflachentexturenbeim Walzen von a-Eisen," Z. Metallkd. **72**, 230–237 (1981).
[42]R. A. Dunlap, *The Mossbauer Effect* (IOP publishing Ltd., 2019).
[43]A. Lisfi and J. C. Lodder, "Relation between the microstructure and magnetic properties of $BaFe_{12}O_{19}$ thin films grown on various substrates," J. Magn. Magn. Mater. **242–245**, 391–394 (2002).

Supplementary material for "Corroborating the magnetic easy axis of epitaxial (100) α-iron and (0001) BaFe12O19 thin films by 57Fe Mössbauer spectroscopy"

Y. E. Li,[1] J. Shine,[2] C. Guguschev,[3] M. Brützam,[3] D. G. Schlom,[1,3,4] and N. Ravi[2]

[1]Department of Materials Science and Engineering, Cornell University, Ithaca, New York 14853, USA

[2]Physics Department, Spelman College, Atlanta, Georgia 30314, USA

[3]Leibniz-Institut für Kristallzüchtung, Max-Born-Str. 2, 12489 Berlin, Germany

[4]Kavli Institute at Cornell for Nanoscale Science, Ithaca, New York 14853, USA

Contact:

[1]schlom@cornell.edu, [2]nravi@spelman.edu

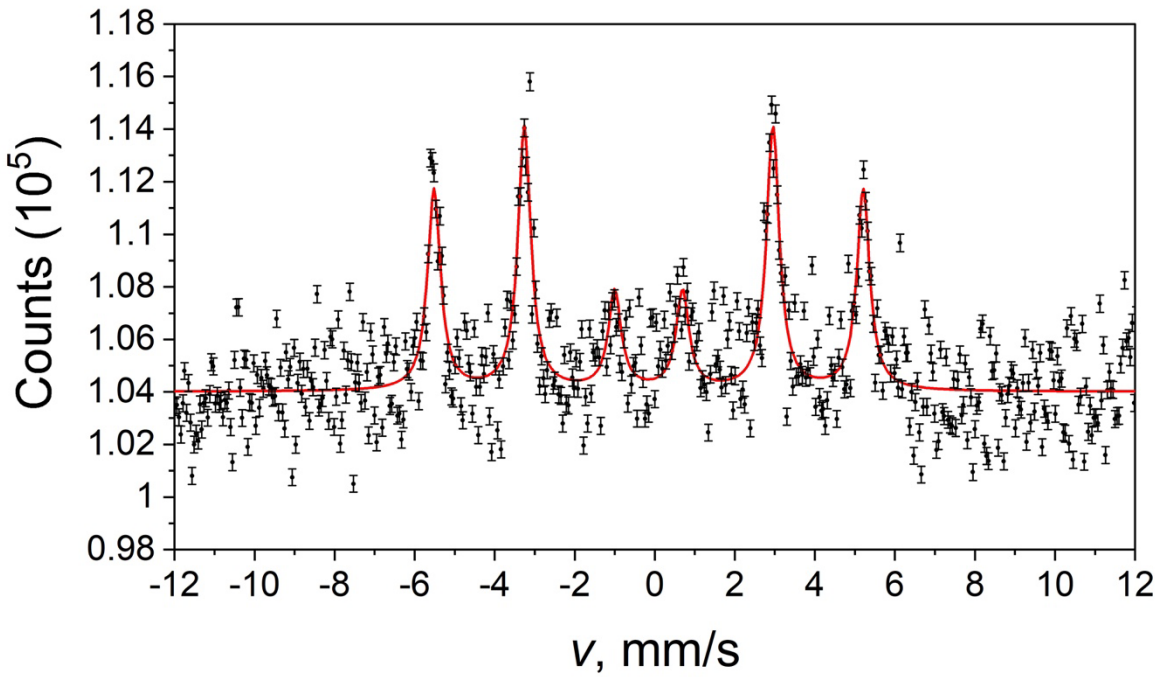

Figure S1. CEMS data of a rolled Fe-foil of 30 μm thickness.